Ocean Engineering 250 (2022) 110579

Contents lists available at ScienceDirect

Ocean Engineering

journal homepage: www.elsevier.com/locate/oceaneng

Impact of cyclic strain accumulation on the tilting behaviour of monopiles in sand: An assessment of the Miner's rule based on SANISAND-MS 3D FE modelling

Haoyuan Liu [a,*], Federico Pisanò [b], Hans Petter Jostad [a], Nallathamby Sivasithamparam [a]

[a] Norwegian Geotechnical Institute, Sognsveien 72, Oslo 0806, Norway
[b] Faculty of Civil Engineering and Geosciences, Delft Univ. of Technology, 2628 CN, Delft, Netherlands

ARTICLE INFO

Keywords:
Monopile
Cyclic accumulation
Loading history
Accumulated rotation
Finite element

ABSTRACT

Offshore monopiles accumulate permanent tilt under long-lasting cyclic environmental loads. Accurate prediction of monopile tilt is key to assessing their serviceability, and requires a fundamental understanding of loading history effects. While both experimental and numerical studies are shedding light on this matter, this work uses step-by-step implicit 3D FE modelling to investigate loading history effects in the response to cyclic lateral loading of monopiles in sand and to identify links between local soil behaviour and relevant features of global pile behaviour. For this purpose, the recently developed SANISAND-MS model is adopted to achieve a reliable simulation of sand's cyclic ratcheting. In particular, the validity of an up-scaled Miner's rule for monopile tilting under multi-amplitude cyclic loading is assessed based on the results of 3D FE parametric analyses, with emphasis on the role played by the engineering idealisation of random environmental loading. The validity of such a rule has been numerically investigated both in terms of local soil element response and global foundation behaviour — for the particular case of a large-diameter monopile. In respect, the effect of the loading history idealisation is presented, and it is concluded that Miner's rule does not always rigorously apply to all the cases considered herein. The translation of irregular loading histories into a regular version with loading packages sorted in ascending amplitude order is shown to be a reasonable approach, at least when the possibility of cyclic pore pressure build-up is disregarded.

1. Introduction

Monopile foundations for offshore wind turbines (OWTs) must be designed to guarantee that the superstructure remains fully functional through the whole lifetime environmental cyclic loading. In this regard, avoiding the excessive cyclic accumulation of lateral monopile tilt is extremely relevant to design (Arany et al., 2015), as is also testified by the growing body of offshore geotechnical research dedicated to the subject (Cuéllar et al., 2009; LeBlanc et al., 2010b; Klinkvort and Hededal, 2014; Byrne et al., 2015; Staubach and Wichtmann, 2020).

The tilting response of monopiles is affected by a number of governing factors, including monopile geometry, soil type, and loading conditions. The influence of these factors has been investigated experimentally by several authors, mostly with regard to the drained cyclic response of monopiles in sand (LeBlanc et al., 2010a; Klinkvort and Hededal, 2013; Richards et al., 2019). Relevant numerical modelling research has also been carried out, most often to develop simplified engineering methods for the serviceability and fatigue analysis of monopiles — see, e.g., the 0D macroelement models proposed by Houlsby et al. (2017) and Page et al. (2018), as well as Abadie et al. (2019, 2020).

Recently, three-dimensional finite element (3D FE) simulations have been increasingly adopted to explore the fundamental mechanisms that govern monopile tilting (Jostad et al., 2020; Liu et al., 2021), also with respect to the effects of the monopile installation method (Staubach et al., 2020; Fan et al., 2021; Bienen et al., 2021). The 3D FE analysis of cyclic soil–monopile interaction can be built on either 'explicit' or 'implicit' constitutive modelling of cyclic soil behaviour. 'Explicit' modelling takes the number of loading cycles as a model input to compute monopile deformation over a given loading period (Achmus et al., 2009; Jostad et al., 2014; Wichtmann et al., 2017). In such a way, the accumulated soil strains over each loading cycle are exclusively evaluated at one selected time. Generally, extensive experimental programmes are required to support explicit modelling calculations. In contrast, 'implicit' methods compute the cyclic soil response incrementally, i.e., in a step-by-step manner, so that the overall behaviour of

* Corresponding author.
E-mail addresses: haoyuan.liu@ngi.no (H. Liu), F.Pisano@tudelft.nl (F. Pisanò), hans.petter.jostad@ngi.no (H.P. Jostad), nallathamby.siva@ngi.no (N. Sivasithamparam).

https://doi.org/10.1016/j.oceaneng.2022.110579
Received 28 November 2021; Accepted 6 January 2022
Available online 14 March 2022

the considered system is obtained as a result of usual time integration. Nowadays, 'implicit' 3D FE modelling approaches are being increasingly adopted to study the cyclic performance of monopile lateral behaviour under cyclic loading (Cuéllar et al., 2014; Tasiopoulou et al., 2021; Liu et al., 2021; Liu and Kaynia, 2021).

Most of the abovementioned experimental and computational studies exclusively consider monopiles subjected to regular, single-amplitude cyclic loading histories. However, real environmental loads occur in irregular repetitions with varying amplitude, average level, and frequency. In offshore design practice, irregular loading histories are often idealised as regular using methods such as the *rainflow counting* method (Kaggwa et al., 1991), which leads to convert the original loading history into a sequence of multiple loading packages with cyclic amplitude and number of cycles varying from one package to the next. While more research on the response of monopiles to multi-amplitude loading cycles is certainly needed (Page et al., 2021), the well-known Miner's rule has been often adopted to conceptualise loading history effects in the tilting response of monopiles. Miner's rule is an empirical postulate that was originally proposed to describe cyclic fatigue mechanisms in metals (Miner et al., 1945; Wilkins, 1956), and later applied to cyclically loaded soils as well (Stewart, 1986; Wichtmann et al., 2010). However, the upscaling of Miner's rule from the soil element level to the global foundation scale level can only be accomplished through further studies on the response of offshore foundations to multi-amplitude cyclic loading, with focus on the implications of adopting idealised/regular loading histories for engineering design purposes. Currently, the studies on this aspect have been mainly performed mainly on 1 g experimental (LeBlanc et al., 2010a; Abadie et al., 2018; Luo et al., 2020; Ma et al., 2021) and 'explicit' 3D FE modelling (Wichtmann et al., 2017) perspectives.

The present study builds on 'implicit' 3D FE modelling of cyclic monopile–sand interaction, in which the quality of the soil constitutive model plays a crucial role. In this regard, the SANISAND-MS model with ratcheting control proposed by Liu et al. (2019) is adopted herein to perform parametric studies on the response of monopiles to multi-amplitude cyclic loading. Using advanced constitutive models in 3D FE simulations allows to study in detail geotechnical mechanisms that force-resultant macro-models can only incorporate as a *priori* constitutive assumptions (Abadie et al., 2018). Similar considerations apply to the 'meso-scale' SANISAND-MS model, whose formulation and calibration could be supported by parallel micro-mechanical studies (Alonso-Marroquin and Herrmann, 2004; Kawamoto et al., 2018). In what follows, the ability of SANISAND-MS to simulate at the soil element level a cyclic behaviour that is compliant with Miner's rule is first explored in Section 2. The upscaling of Miner's rule to the global monopile scale is then discussed based on 3D FE results presented in Section 3 in terms of cyclic pile head displacement, shear force and moment distributions, and lateral soil reactions (i.e., $p - y$ response). The implications of idealising the external loading history are discussed in Section 4 with respect to two different cases, in which realistic loading histories of 1 h and 20 min duration are considered in their original and idealised versions. The ultimate goal of this work is to exploit state-of-the-art 3D FE modelling to investigate relevant loading history effects in the cyclic lateral response of monopiles. The results and observations presented in the following will provide further insight into lesser-known aspects of cyclic soil–pile interaction, and will support the enhancement of existing simplified methods for engineering analysis/design.

2. SANISAND-MS modelling of cyclic sand behaviour

2.1. Model highlights

SANISAND-MS model is an elasto-plastic implicit constitutive model, originally proposed by Liu et al. (2019) to improve the simulation of cyclic sand ratcheting with respect to the previous SANISAND parent model by Dafalias and Manzari (2004). The model is formulated in the framework of bounding surface plasticity, and complies with well-established critical state principles through the use of the state parameter introduced by Been and Jefferies (1985), which allows to capture the dependence of sand's behaviour both on current void ratio and mean effective stress. Following the work of Corti et al. (2016), the 'memory surface' concept has been introduced into the SANISAND constitutive formulation to enhance the simulation of cyclic strain accumulation, i.e., to control the development of cyclic ratcheting. As is shown in Fig. 1, SANISAND-MS features four main model surfaces – namely, bounding, yield, dilatancy and memory surfaces – and has been quantitatively validated against experimental data from the literature — more details about model formulation and validation may be found in Liu et al. (2019), Liu and Pisanò (2019) and Liu et al. (2020). The applicability of the resulting 3D FE SANISAND-MS framework to the analysis of cyclically loaded monopiles has been recently demonstrated by Liu et al. (2021) and Liu and Kaynia (2021), though with exclusive reference to single-amplitude loading cycles.

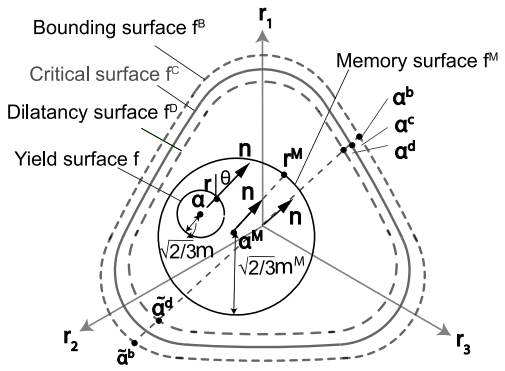

Fig. 1. SANISAND-MS model loci.

2.2. Model performance under multi-amplitude loading: compliance with Miner's rule at soil element level

It is customary in geotechnical research to validate cyclic constitutive models against laboratory test results obtained under single-amplitude repeated loading. However, soils under offshore foundations are normally subjected to highly irregular, non-stationary cyclic loads, whose impact on the interpretation and modelling of cyclic soil behaviour is still an open research question (Andersen, 2015; Zografou et al., 2018). This section provides new evidence about the performance of SANISAND-MS under multi-amplitude cyclic loading. In particular, compliance with the above mentioned Miner's rule is verified to expand the validation basis of the model, and boosts confidence in its use for the solution of geotechnical boundary value problems. Miner's rule has been proposed to estimate the cumulative fatigue damage of metals using an linear accumulation approach. The rule can be expressed using the equation below:

$$f_D = \sum_{i=1}^{k} \frac{n_i(\sigma_i^{ampl})}{N_i(\sigma_i^{ampl})} \tag{1}$$

where f_D is the total damage that can be set as one (i.e., failure) for design purpose. N_i is the total number of cycles to failure when subjected to a constant amplitude σ_i^{ampl}; and n_i is the number of the applied load cycles under the same load amplitude. Miner's rule is a linear damage rule that assumes the effects of the sequence of applied load amplitudes can be ignored. Focusing on the design aspects of accumulation of foundation displacement (and thus accumulation of the strain in local soil response), the essence of Miner's rule in relation to sand's cyclic behaviour can be summarised by the following two statements:

Table 1
SANISAND-MS model parameters for the Karlsruhe sand tested by Wichtmann et al. (2010). Compared to the original calibration in Liu et al. (2019), μ_0 was reduced from 260 to 200 for better simulation of longer loading histories (i.e., number of cycles $N = 10^5$, instead of $N = 10^4$)

Elasticity		Critical state					Yield surface	Plastic modulus			Dilatancy		Memory surface		
G_0	ν	M	c	λ_c	e_0	ξ	m	h_0	c_h	n^b	A_0	n^d	μ_0	ζ	β
110	0.05	1.27	0.712	0.049	0.845	0.27	0.01	5.95	1.01	2.0	1.06	1.17	200	0.0005	1

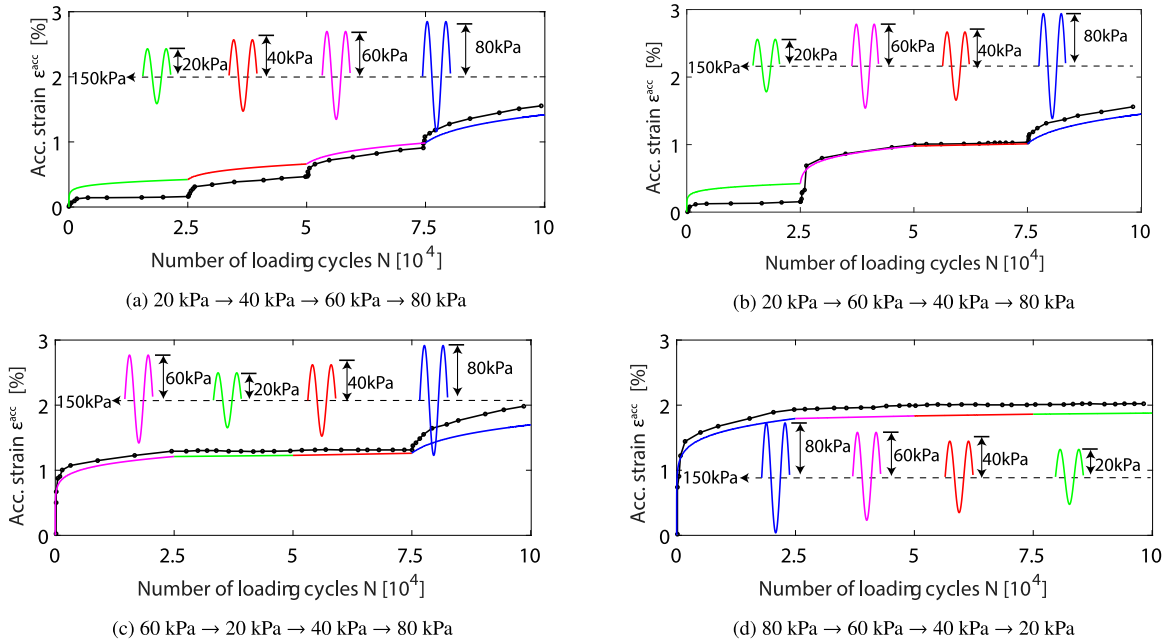

(a) 20 kPa → 40 kPa → 60 kPa → 80 kPa

(b) 20 kPa → 60 kPa → 40 kPa → 80 kPa

(c) 60 kPa → 20 kPa → 40 kPa → 80 kPa

(d) 80 kPa → 60 kPa → 40 kPa → 20 kPa

Fig. 2. Strain accumulation patterns under different cyclic load sequences. Triaxial test settings: q^{ave} = 150 kPa, p_{in} = 200 kPa, e_{in} = 0.698 (D_r = 59%). Comparison between experimental data from (Wichtmann et al., 2010) (dotted black lines) and SANISAND-MS results (solid lines in colour). (For interpretation of the references to colour in this figure legend, the reader is referred to the web version of this article.)

1. accumulation of irreversible plastic strains is only possible when the current cyclic load amplitude is the highest ever experienced by the material;
2. given a cyclic loading history formed by segments (or packages) of different amplitude, the specific sequence of such packages has only minor influence on the plastic strains finally accumulated (residual strains).

In order to validate SANISAND-MS from a Miner's rule standpoint, the results of multi-amplitude, high-cyclic triaxial tests reported by Wichtmann et al. (2010) were numerically simulated. The original laboratory tests were performed on dry, medium-coarse Karlsruhe sand (D_{50} = 0.55 mm, D_{10} = 0.29 mm, e_{max} = 0.874, e_{min} = 0.577, maximum (dry) unit weight γ_{max} = 16.5 kN/m^3, minimum (dry) unit weight γ_{min} = 13.9 kN/m^3, coefficient of uniformity $C_u = D_{60}/D_{10}$ = 1.8). The corresponding SANISAND-MS model parameters were previously identified by Liu et al. (2019) with respect to single-amplitude cyclic loading conditions (see Table 1).

All the results considered in the following, both experimental and numerical, are associated with the following triaxial test settings: p_{in} = 200 kPa (mean stress at the beginning of, and during, cyclic loading), q^{ave} = 150 kPa (average deviatoric stress during cyclic loading), and initial, pre-cyclic relative density set to D_r = 59% (e_{in} = 0.698, initial void ratio) in numerical simulations to represent the experimental range of 58%–63%. The soil response to cyclic load packages of four different deviatoric stress amplitude (q^{ampl} = 20, 40, 60, 80 kPa) was considered with respect to the following load sequences (Fig. 2):

(a) 20 kPa → 40 kPa → 60 kPa → 80 kPa;
(b) 20 kPa → 60 kPa → 40 kPa → 80 kPa;
(c) 60 kPa → 20 kPa → 40 kPa → 80 kPa;
(d) 80 kPa → 60 kPa → 40 kPa → 20 kPa.

For each sequence, the accumulated total strain ε^{acc} was recorded at the end of each cycle when $q = q^{ave}$, without accounting for the very first cycle:

$$\varepsilon^{acc} = \sqrt{\left(\varepsilon_a^{acc}\right)^2 + 2\left(\varepsilon_r^{acc}\right)^2} \tag{2}$$

where ε_a and ε_r denote the axial and radial strain components – see also Wichtmann et al. (2010) and Liu et al. (2019).

Fig. 2 shows a generally good agreement between experimental and SANISAND-MS results over the 10^5 cycles considered in the testing programme (4 packages comprising 25 000 cycles each). In particular, Fig. 2a displays gradual monotonic increase in ε^{acc} with the number of cycles N, at a rate depending on the current cyclic load amplitude. In Fig. 2b obvious strain accumulation occurs during the second package (q^{ampl} = 60 kPa), at a rate faster than observed during the first segment of lower amplitude (q^{ampl} = 20 kPa); the lower cyclic load in the third stage leads to practically no ratcheting, finally re-activated by the highest load amplitude in the fourth package. Strain accumulation patterns fully consistent with Miner's rule/statement 1 can also be observed for the third (Fig. 2c) and fourth (Fig. 2d) load sequences. The last case in Fig. 2d corroborates the idea of cyclic strain accumulation being dominated by the highest load amplitudes, as they are experienced by the soil for the first time.

The results in Fig. 2, however, do not seem to fully confirm the validity of Miner's rule/statement 2. Both the experimental and simulation results indicate that applying load packages with large amplitude results in larger accumulated strain. The experimental results in Figs. 2c and 2d indicate the achievement of an accumulated strain equal to 2% after 10^5 cycles, which is larger than the final value of ~1.7% that is visible in Figs. 2a and 2b. Although $\varepsilon^{acc} - N$ trends are specific to the considered load sequence (which challenges the general validity of Miner's rule), the residual strain $\varepsilon^{acc}\left(N = 10^5\right)$ lies in all cases within

a relatively narrow range, i.e., 1.7~2.0%. It may thus be argued that the specific arrangement of the cyclic packages may only have a weak impact on $\varepsilon^{acc}\left(N=10^5\right)$. In other words, only a few, high-amplitude packages seem to affect soil ratcheting in the longest term. Fig. 2 support the application of SANISAND-MS to cyclic soil–structure interaction problems involving multi-amplitude cycles, with soil parameters that can still be calibrated against more common single-amplitude test data.

3. Upscaling of Miner's rule

After evaluating the compliance with Miner's rule of SANISAND-MS simulations performed at the soil element level (Fig. 2), this section aims to assess whether the rule may be upscaled to monopile–sand systems subjected to multi-amplitude lateral cyclic loading. While the validity of such upscaling has been recently supported by several experimental studies (Li et al., 2015; Truong et al., 2019; Abadie et al., 2018), the rest of this work will seek further insight using SANISAND-MS 3D FE modelling.

3.1. 3D FE model

All the results presented in the following have been obtained using the OpenSees FE simulation platform (McKenna, 2011), within which an original implementation of SANISAND-MS was previously developed (Liu et al., 2019). Fig. 3 shows the 3D FE model adopted in this study, which features:

(1) an elastic tubular monopile, with diameter $D = 5$ m, embedded length $L = 20$ m, and wall thickness $t = 10$ cm;
(2) a soil box domain with dimensions $W_1 = 30$ m, $W_2 = 35$ m, $L+B = 30$ m, as indicated in Fig. 3. The symmetry of the problem at hand (one-directional lateral loading) was exploited to reduce the computational costs, so that only half of the soil domain was modelled;
(3) the soil is assumed to be dry (fully drained conditions) and characterised by the SANISAND-MS parameters given in Table 1. Initial values of relative density equal to $D_r = 30\%$ and $D_r = 70\%$ are exclusively considered in the following;
(4) lateral load H applied with an eccentricity $e_{ecc} = 4D = 20$ m above the soil surface. The load application point was connected at the mudline with the rest of the 3D pile by means of an elastic Timoshenko beam. Boundary conditions were imposed on the soil domain to obtain a fully fixed bottom surface, a free upper surface, and no horizontal displacement along the direction perpendicular to the lateral surface. Detailed description of FE solution algorithms and model verification are provided by Liu et al. (2021).

3.2. Simulation programme with multi-amplitude regular cyclic loading

A first set of SANISAND-MS 3D FE simulations was performed to investigate the response of the reference monopile to multi-amplitude regular cyclic loading, i.e., under a sequence of different cyclic load packages of different, though constant, amplitude. As is shown in Fig. 4, each cyclic load package is completely defined by its average amplitude (H_{ave}) and regular cyclic variation (H_{cy}). Alternatively, the dimensionless amplitude and asymmetry load factors introduced by LeBlanc et al. (2010a)) – ζ_b and ζ_c, respectively – may be also be used after defining a reference horizontal load H_{ref} (here taken as the horizontal load that monotonically induces a lateral pile displacement at the soil surface equal to $0.1D$):

$$\zeta_b = H_{max}/H_{ref} = (H_{ave} + H_{cy})/H_{ref} \tag{3}$$

$$\zeta_c = H_{min}/H_{max} = (H_{ave} - H_{cy})/(H_{ave} + H_{cy}) \tag{4}$$

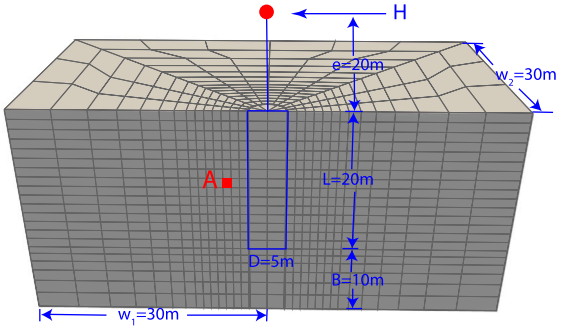

Fig. 3. 3D FE model of a laterally loaded monopile in sand. The reference soil element A is located 9.3 m under the ground surface, at a distance of 2.1 m from the monopile shaft.

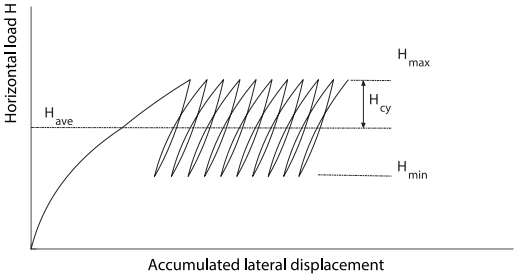

Fig. 4. Definition of cyclic load components.

where H_{max} and H_{min} denote the maximum and minimum lateral load values during a given cyclic package. Based on Liu et al. (2021), the reference horizontal load for the monopile in Fig. 3 is $H_{ref} = 15\,450$ kN and $H_{ref} = 26\,800$ kN for $D_r = 30\%$ and $D_r = 70\%$, respectively. In this work, the monopile is subjected to packages of pure one-way cyclic loading (i.e., $\zeta_c \geq 0$), with maximum ζ_b never larger than 0.3. A summary of the considered loading cases with regular cyclic packages is provided in Table 2. Load history effects are investigated by simulating different application patterns of the selected load packages, namely with increasing, mixed, and decreasing amplitude. Due to the computational costs that are typical of implicit 3D FE calculations, individual packages of 100 cycles each are exclusively considered: while this limitation should be carefully borne in mind prior to any extension to real environmental loading histories, it will still be possible to infer useful lessons about cyclic soil–monopile interaction under relatively complex lateral loading sequences.

3.3. Load history effects on global monopile cyclic response

Several numerical studies on OWTS foundation behaviour under cyclic loading of constant amplitude have been recently published for both cases of drained (Staubach and Wichtmann, 2020; Tasiopoulou et al., 2021; Staubach et al., 2021; Liu et al., 2021) and undrained (Tasiopoulou et al., 2021; Liu and Kaynia, 2021) conditions. This section adds to the understanding of cyclic monopile behaviour by investigating the load history effects associated with the application of regular multi-amplitude cyclic load sequences.

3D FE results indicate the monopile lateral displacement (unless otherwise specified, always referred to the value at the soil surface level) evolves at a significant rate when the current load amplitude is the highest experienced until that moment — for each cycle, the respective pile lateral displacement is the value associated with the average load level ($H = H_{ave}$). This is clearly visible for the simulation cases in loose sand ($D_r = 30\%$) – see Figs. 5a and 6a – where the increasing cyclic amplitude of subsequent load packages induces progressively

Table 2
Regular multi-amplitude cyclic loading cases for the reference monopile in loose and dense sand.

Order	D_r [%]	H_{ref} [kN]	H_{ave} [kN]	H_{cy} [kN]	ζ_b	ζ_c
Increasing				770 → 1540 → 2310	0.2 → 0.25 → 0.3	0.5 → 0.21 → 0
Mixed	30	15 450	2310	1540 → 770 → 2310	0.25 → 0.2 → 0.3	0.21 → 0.5 → 0
Decreasing				2310 → 1540 → 770	0.3 → 0.25 → 0.2	0 → 0.21 → 0.5
Increasing				1340 → 2680 → 5020	0.2 → 0.25 → 0.3	0.5 → 0.21 → 0
Mixed	70	26 800	4020	2680 → 1340 → 4020	0.25 → 0.2 → 0.3	0.21 → 0.5 → 0
Decreasing				4020 → 2680 → 1340	0.3 → 0.25 →0.2	0 → 0.21 → 0.5

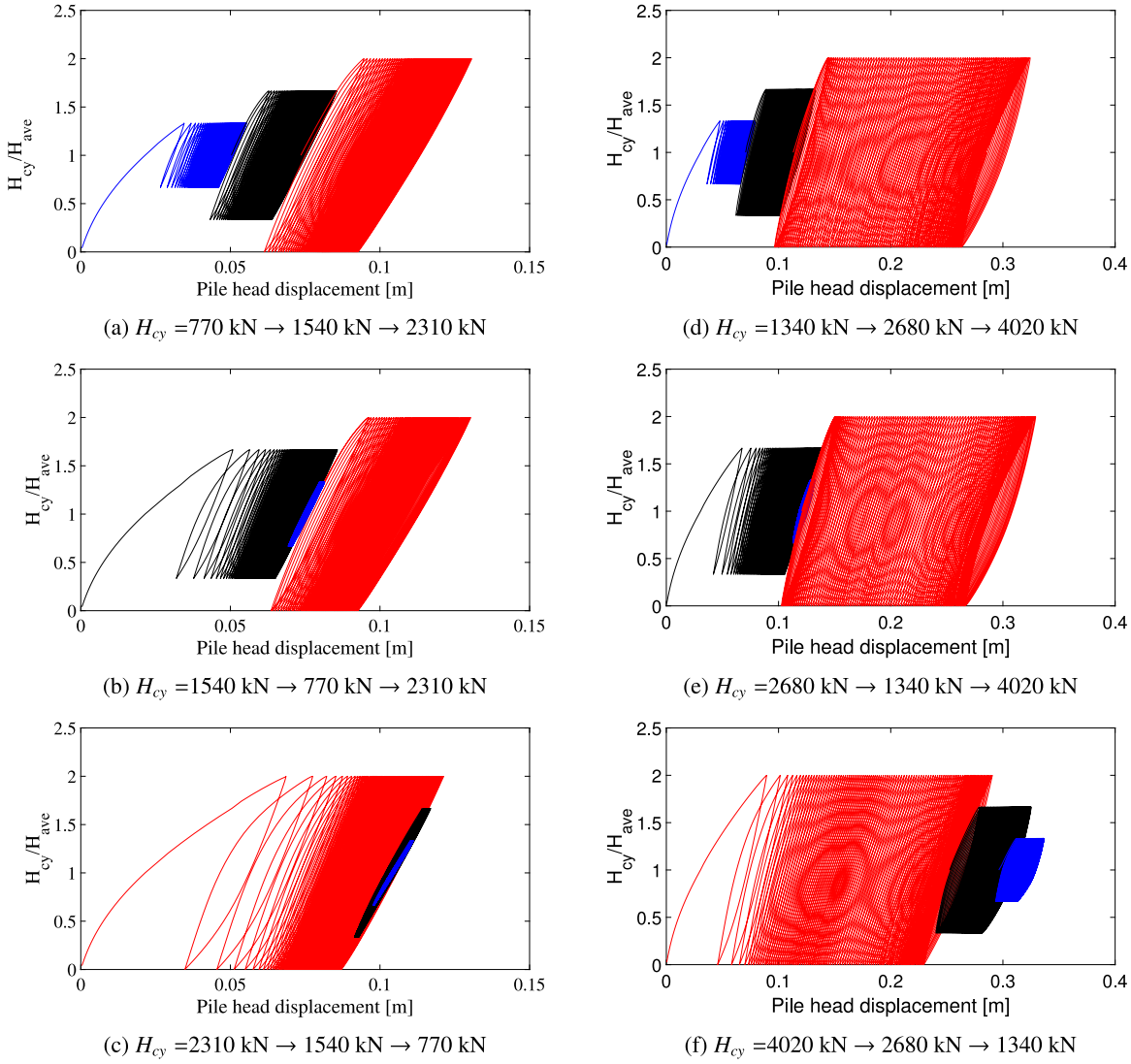

(a) H_{cy} =770 kN → 1540 kN → 2310 kN
(d) H_{cy} =1340 kN → 2680 kN → 4020 kN
(b) H_{cy} =1540 kN → 770 kN → 2310 kN
(e) H_{cy} =2680 kN → 1340 kN → 4020 kN
(c) H_{cy} =2310 kN → 1540 kN → 770 kN
(f) H_{cy} =4020 kN → 2680 kN → 1340 kN

Fig. 5. Influence of the cyclic loading sequence on the evolution of monopile tilt — force–displacement response at the pile head. (a)–(c), H_{ave} = 2310 kN, D_r = 30%; (d)–(f), H_{ave} = 4020 kN, D_r = 70%.

higher lateral displacement accumulation rates. Conversely, negligible lateral displacement is observed in Figs. 5c and 6c for the second and third packages, both featuring an amplitude smaller than the first. The intermediate case in Figs. 5b–6b also shows displacement accumulation trends in full agreement with an up-scaled version of Miner's rule.

Qualitatively similar results have also been obtained for the case of dense foundation sand (D_r = 70%): (1) when increasing the cyclic amplitude through the subsequent load packages, the lateral displacement of the pile head accumulates significantly from package to package (see Figs. 5d and 6d); (2) Figs. 5e and 6e show again displacement accumulation trends in full agreement with an upscaled Miner's rule; (3) if the loading package of largest cyclic amplitude is applied first, a lower pile head displacement accumulation rate results for the following packages — see Figs. 5f and 6f.

It is worth noting in Figs. 5f and 6f that, although with an accumulation rate that is much lower than during the second and third packages, non-negligible pile tilting still occurs during the last weakest package. Such phenomenon has also been experimentally observed by Barari et al. (2017). One possible reason is that for dense sand, notwithstanding the assumption of drained conditions in this work, many element are sheared under (nearly) constant volume conditions — thus mobilising a soil response that may be referred to as of an 'undrained-type', as indicated by Fig. 7c. During this process, soil shear straining develops until its strain-saturation state (Fig. 7d). The continually developing pile deflection may be a direct consequence of

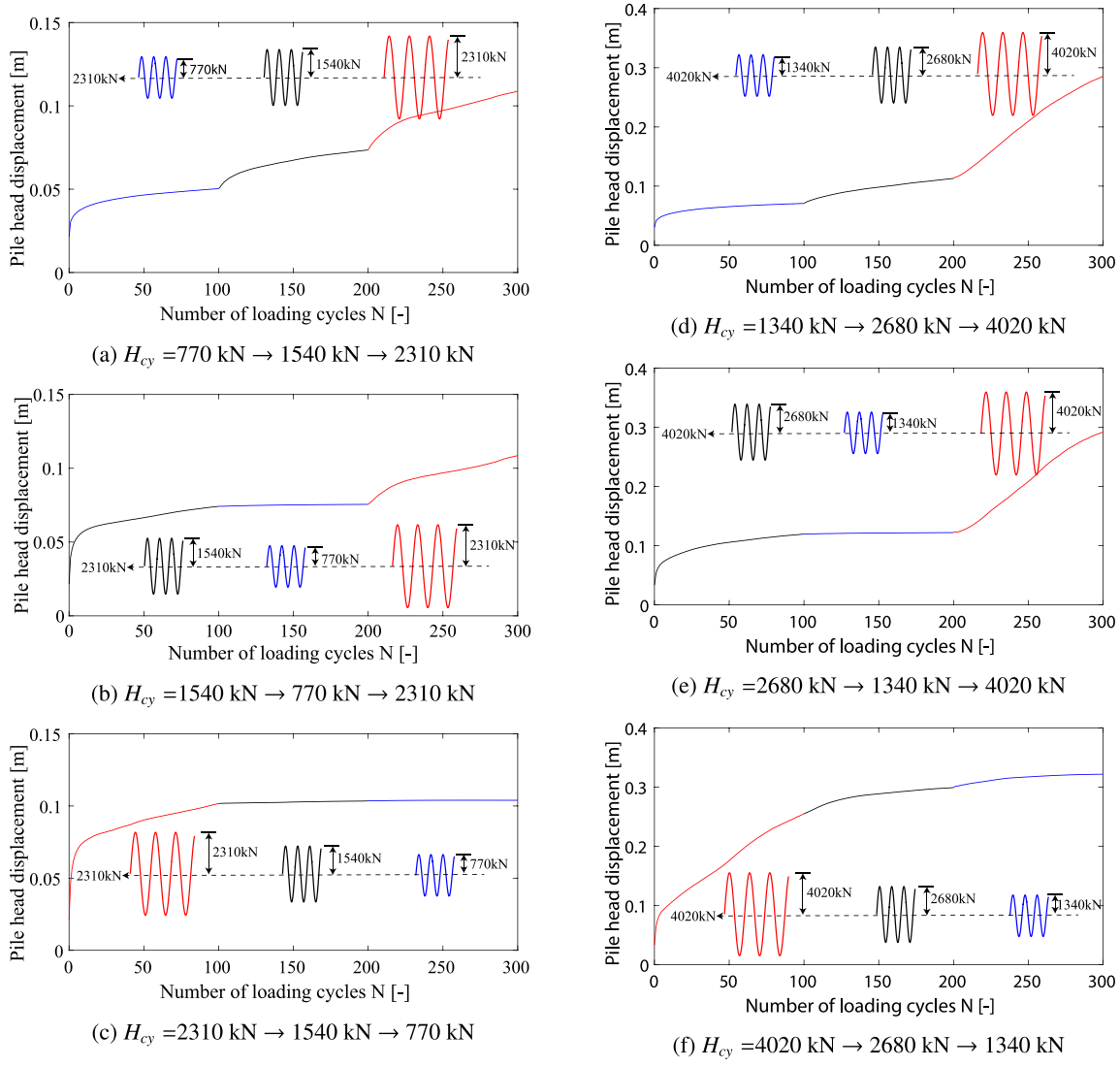

Fig. 6. Influence of the cyclic loading sequence on the evolution of monopile tilt — pile head lateral displacement against the number of loading cycles. (a)–(c), H_{ave} = 2310 kN, D_r = 30%; (e)–(f), H_{ave} = 4020 kN, D_r = 70%.

the shear/deviatoric strain evolution of surrounding soil. However, in loose sand, the stress evolution in most elements reaches a steady state at a moderate p level (Fig. 7c), while both the volumetric and shear strains evolve only slightly (Fig. 7b).

With regard to the considered loading sequences, the values of accumulated lateral displacement after 300 cycles are not exactly identical but lie within a very narrow range (i.e., within 0.105~0.11 m for loose sand and 0.29~0.32 m for dense sand) without an obvious dependence on the specific package application sequence. Such conclusion agrees with the experimental (1 g, pile) observations from LeBlanc et al. (2010a) and Ma et al. (2021). However, one may notice that for other foundation type (e.g., suction caisson as studied by Luo et al. (2020)), loading history with parcels in the order of decreasing cyclic amplitude results in larger accumulated displacement/rotation.

Comparing the accumulated pile head displacement in all three loading histories (parcels with increasing, mix and decreasing amplitude), simulation results of loose sand case show less obvious variation than that of dense sand case. It indicates that dense sand is more sensitive to the load sequence (as also observed by Barari et al. (2017)).

The different pile head displacement accumulation patterns in Figs. 5 and 6 indicate, for monopiles both in loose and dense sand, that an upscaled Miner's idealisation may only be partially valid.

Distributions of internal shear force along the monopile are plotted in Figs. 8a and 9a for the cases of D_r = 30% and D_r = 70%, respectively — for all cyclic sequences in Table 2, shear forces values are associated with the last cycle in each loading package when $H = H_{max} = H_{ave} + H_{cy}$. In all instances, the absolute value of the shear force tends to decrease down to about three-quarters of the pile embedded length, which approximately coincides with the location of the monopile rotation point. For a given sand relative density, (nearly) the same shear force distribution is simulated in relation to a certain maximum load amplitude, which confirms the expected dominance of general equilibrium requirements over loading history effects. The corresponding bending moment distributions are presented in Figs. 8b and 9b for D_r = 30% and D_r = 70%, respectively. Similar observations are again applicable to the displayed moment profiles, particularly about the weak impact of the cyclic loading sequence on the calculated bending moment distribution.

In addition to Figs. 8–9, the profiles of shear force bending moment associated with the average load level ($H = H_{ave}$) are displayed in Fig. 10 (D_r = 30%) and Fig. 11 (D_r = 70%) for the last cycle (N = 100) of each load package. In the case of monopile in loose sand (Fig. 10), almost identical distributions of shear force and bending moment result for three considered loading sequences (Table 2), which confirms the validity of the upscaled Miner's rule for the reference

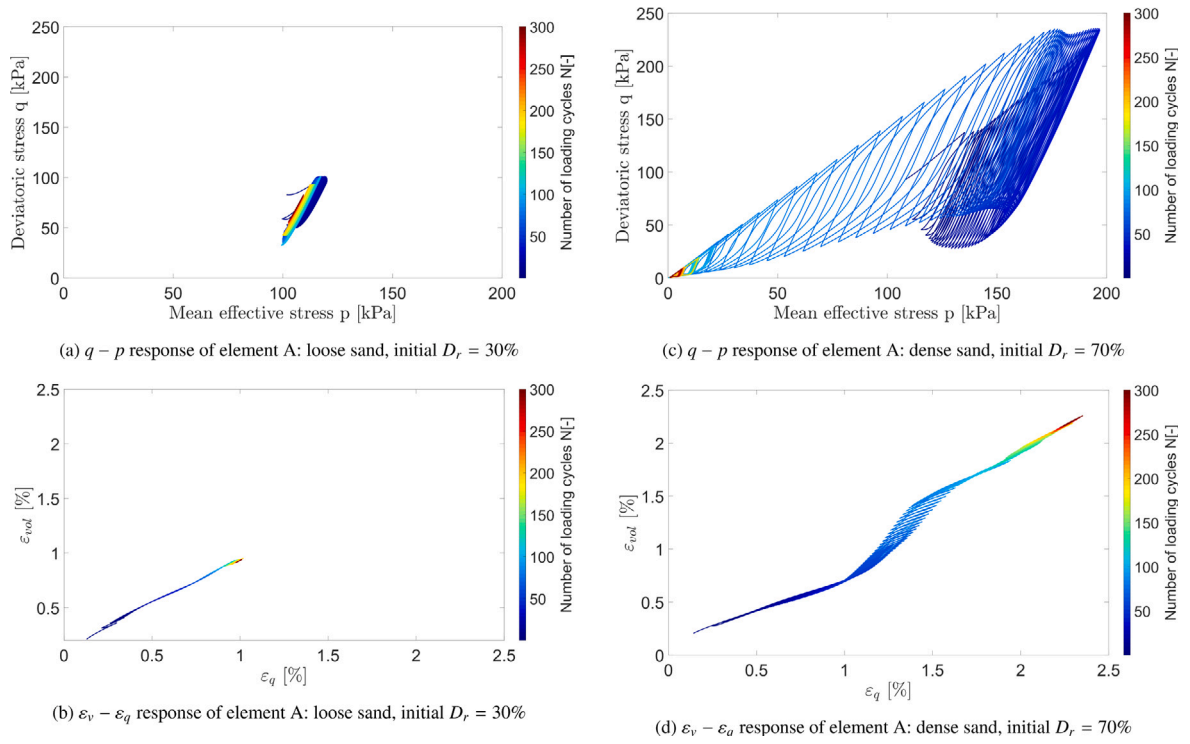

(a) $q - p$ response of element A: loose sand, initial $D_r = 30\%$

(c) $q - p$ response of element A: dense sand, initial $D_r = 70\%$

(b) $\varepsilon_v - \varepsilon_q$ response of element A: loose sand, initial $D_r = 30\%$

(d) $\varepsilon_v - \varepsilon_a$ response of element A: dense sand, initial $D_r = 70\%$

Fig. 7. Stress path evolution (deviatoric stress q against mean effective stress p response) and strain evolution (plastic volumetric strain ε_{vol} against ε_q response). Simulation results on element A in Fig. 3.

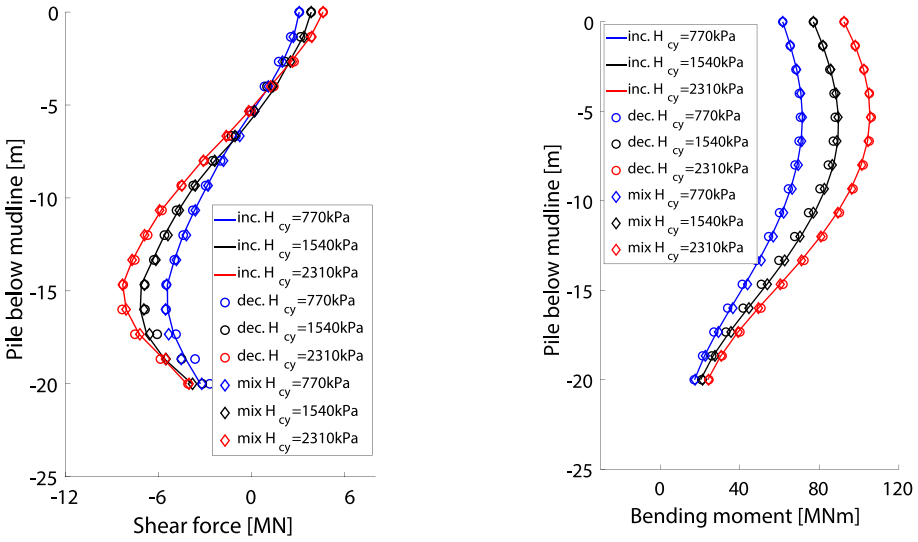

(a) Shear force

(b) Bending moment

Fig. 8. Influence of the cyclic loading sequence on the distributions of (a) shear force and (b) bending moment along the monopile – $D_r = 30\%$. For the three loading sequences in Table 2, results extracted at the end of each load package ($N = 100$) at the correspond maximum load level ($H = H_{max}$).

monopile in loose sand — cf. to Figs. 5a–5c and Figs. 6a–6c: it may thus be suggested that, for the considered loading condition ($\zeta_b \leq 0.3$ and $\zeta_c \geq 0$, drained) and duration ($N = 300$), load history effects are practically negligible in terms of geotechnical and structural response of the monopile. In contrast, the case of dense sand in Fig. 11 reveals shear force and bending moment profiles that are package-dependent when $H = H_{ave}$, with a clear impact of the loading history even though all force/moment profiles are associated with the same external load level on the monopile.

Additional insight into the interaction between monopile and soil may be gained by studying the evolution of the lateral soil reaction at selected depths (integral over the pile circumference) against the pile deflection. Cyclic $p - y$ relationships are shown in Fig. 12 for two representative depths, namely equal to $0.25D$ and $3.5D$ below the soil surface. It may generally be observed that the lateral soil reaction also seems to follow a 'Miner-type' evolution against the pile deflection at the considered depth, as is possible to appreciate in Fig. 5. Substantial variations in lateral soil reaction and pile deflection accumulation are visible at both depths when the load parcel of largest amplitude applied. Slightly larger resistance force is assembled at soil depth = $3.5D$. Overall, very similar soil reaction ranges and pile deflections are obtained for a given D_r, with only minimal loading history effects.

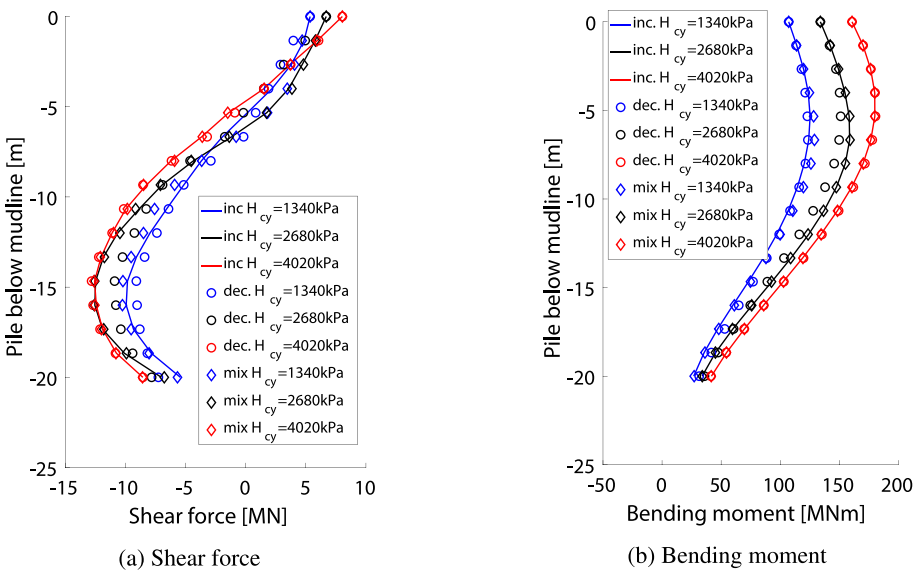

(a) Shear force (b) Bending moment

Fig. 9. Influence of the cyclic loading sequence on the distributions of (a) shear force and (b) bending moment along the monopile – $D_r = 70\%$. For the three loading sequences in Table 2, results extracted at the end of each load package ($N = 100$) at the maximum load level ($H = H_{max}$).

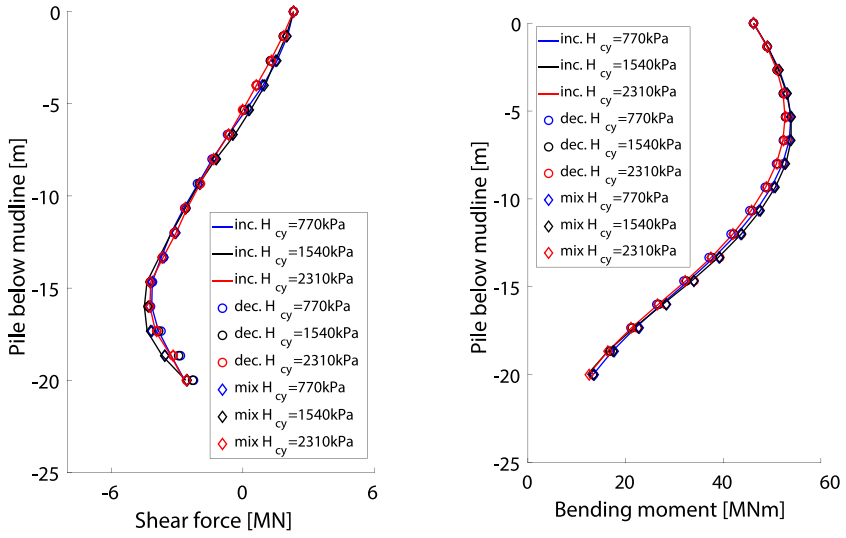

(a) Shear force (b) Bending moment

Fig. 10. Influence of the cyclic loading sequence on the distributions of (a) shear force and (b) bending moment along the monopile – $D_r = 30\%$. For the three loading sequences in Table 2, results extracted at the end of each load package ($N = 100$) at the average load level ($H = H_{ave}$).

3.4. Links to the 'terminal density' concept from 3D FE results

Sandy soils are known to achieve a constant density ('terminal density') when subjected to prolonged cyclic loading (Lackenby et al., 2007). The attainment of a terminal density state depends on the soil initial condition (void ratio, inherit fabric, etc.) and loading/boundary conditions (confining pressure, stress path, etc.). This has been demonstrated through the results of triaxial (Lackenby et al., 2007) and oedometer tests (Park and Santamarina, 2019), and confirmed on a constitutive modelling basis (Liu and Pisanò, 2019).

This section aims to investigate the role of the (mean) effective stress state on sand's 'terminal density' behaviour in the reference boundary value problem – a monopile under lateral cyclic loading. Based on the discussion about Fig. 7d, an obvious evolution of the plastic volumetric strain can still be observed in dense sand under a loading history with load packages ordered in decreasing amplitude order, which means that a trend to approach a terminal density has not been fully triggered in this case. For this reason, the discussion on terminal density in this section is limited to the simulations associated with $D_r = 30\%$.

In Fig. 13, the mechanism behind the 'meso-scale' Miner-type D_r evolution is revealed. The relevance of the soil stress state is highlighted by tracking the evolution of the confining pressure and the Lode angle. In this work, the Lode angle is defined in the range $\theta = [0° \; 60°]$ (from triaxial compression to extension). However, the colour-bar in Fig. 13 is restrained to its real variation range (i.e., 10°~40°) for better visualisation and support to quantitative observations. Plots are associated with a state of the system associated with a load level of $H = H_{ave}$ for each cycle.

Under the three considered loading cases, the relative density D_r of an element keeps evolve on the condition that the mean effective stress p or the Lode angle vary as well. Only when both the mean effective stress p and the Lode angle achieve a relatively stable state (for instance, $N = 50$~100 in Fig. 13a, $N = 100$~200 in Fig. 13b and

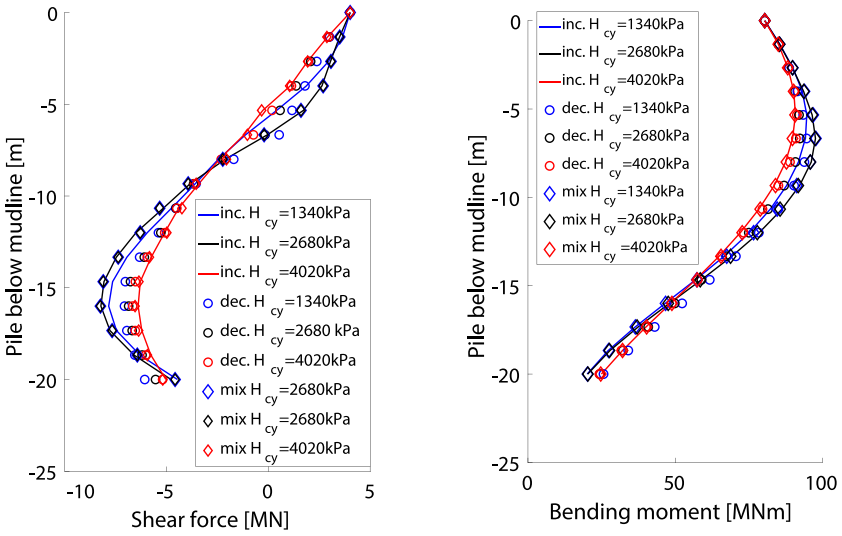

(a) Shear force (b) Bending moment

Fig. 11. Influence of the cyclic loading sequence on the distributions of (a) shear force and (b) bending moment along the monopile – $D_r = 70\%$. For the three loading sequences in Table 2, results extracted at the end of each load package ($N = 100$) at the average load level ($H = H_{ave}$).

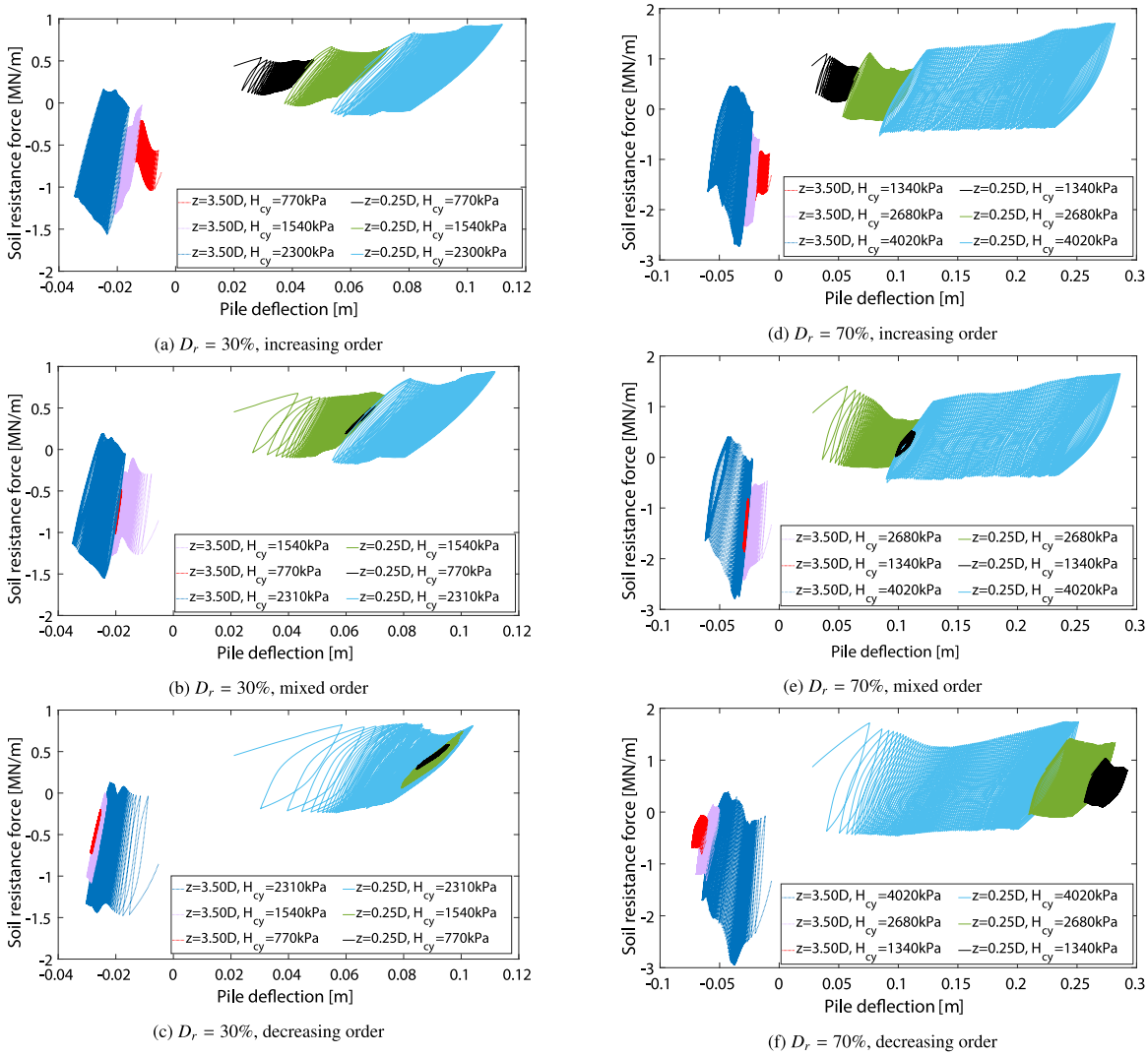

(a) $D_r = 30\%$, increasing order (d) $D_r = 70\%$, increasing order

(b) $D_r = 30\%$, mixed order (e) $D_r = 70\%$, mixed order

(c) $D_r = 30\%$, decreasing order (f) $D_r = 70\%$, decreasing order

Fig. 12. Cyclic soil resistance force against pile deflection under different loading sequences. (a)~(c): $D_r = 30\%$ and (d)~(f) $D_r = 70\%$.

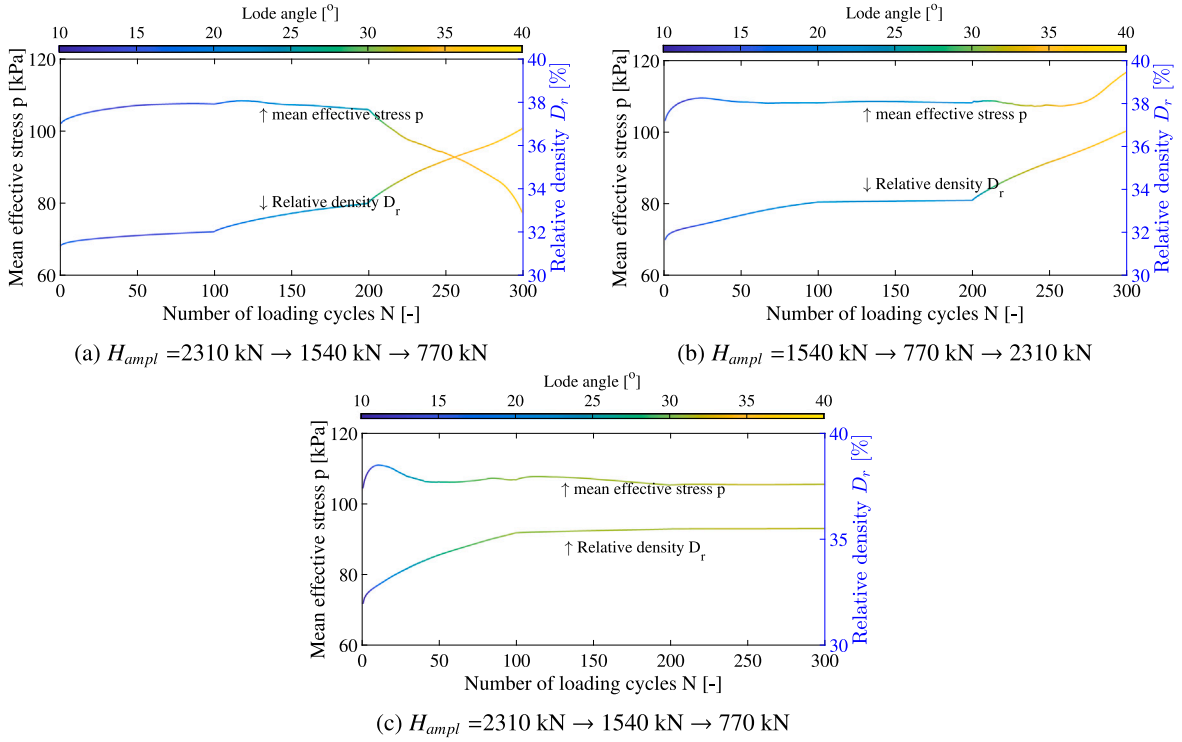

Fig. 13. Relationship between sand relative density and stress conditions. Simulation results on element A in Fig. 3. For all simulations, H_{ave} = 2310 kN, D_r = 30%. (For interpretation of the references to colour in this figure legend, the reader is referred to the web version of this article.)

N = 150~300 in Fig. 13c), D_r ceases to evolve significantly. These simulation results are in further agreement with the notion of 'terminal density', though under stress paths and loading conditions that are more complex than in the aforementioned experimental studies. Apart from confirming the validity of the 'terminal density' concept, a local response consistent with Miner's rule is also exemplified in Fig. 13 in terms of $D_r - N$ trends. These observations lead to regard macro-Miner's rule as a direct consequence of local sand's ratcheting behaviour.

4. Impact of the loading history idealisation

Monopiles are in reality subjected to irregular cyclic loading. In engineering design practice, however, irregular loading is traditionally transformed into idealised regular load parcels characterised by average load levels that are the same for simplification, but with a different arrangement of the load amplitudes — typically with load parcels of uniform amplitude being arranged in ascending amplitude order. After idealising the loading process, it is assumed that the accumulated pile head displacement at the end of the idealised load history is representative of its value under the real irregular loading sequence. To seek confirmation of this assumption, two sets (set A and B, each set contains two load cases) of simulations are performed for the same reference monopile considered so far in dense sand, in combination with the following load histories:

A-1 20 min recorded time domain load history of an offshore wind turbine (extracted from a 1-h storm). The load level is re-scaled so that the maximum load H_{max} = 15.7 MN (it corresponds to $\zeta_b = 0.58$) as a high estimation of a load level.

A-2 the idealised load history transformed from the irregular load history $A-1$ using Rain Flow Counting method (Kaggwa et al., 1991). The idealised load history includes 5 load parcels (324 loading cycles). The average load H_{ave} = 5.4 MN. The amplitude of the load parcels ranges from 1.026 to 10.266 MN. In this way, the maximum load level in $A-2$ is the same as in $A-1$.

B-1 The 1-h load storm (the same as the recorded storm load for $A-1$) with the load level be re-scaled so that H_{max} = 7.6 MN (it corresponds to $\zeta_b = 0.27$).

B-2 the idealised load history transformed from the irregular load history $B-1$ using Rain Flow Counting method. The idealised load history includes 12 load parcels (900 loading cycles). The average load H_{ave} = 3.75 MN. The amplitude of the load parcels ranges from 0.2 to 3.85 MN. In this way, the maximum load level in $B-2$ is the same as in $B-1$.

When translating irregular loading into idealised loading (i.e., from $A-1$ and $B-1$ to $B-1$ and $B-2$), each regular loading cycle has a period of around 4 s.

4.1. Pile head displacement

The simulation cases in this section are limited to monopile behaviour in dense sand only in order to better consider the real life design situation. Pile head lateral displacements obtained from the two sets of loading conditions are plotted in Fig. 14a (load histories $A-1$ and $A-2$, the magnitude of the displacements is associated with the left y-axis of the plot) and Fig. 14b (load histories $B-1$ and $B-2$). For convenient relating of displacement evolution pattern to the changing of loading amplitude, the load histories are also included in the figure (the magnitude is associated with the right y-axis).

Loading history effect is first investigated through the comparison of accumulated displacement at the end of loading histories $A-1$ and $A-2$ – the corresponding load level is about H = 8.8 MN, as indicated in Fig. 14. Monopile subjected to irregular load history $A-1$ accumulates lateral displacement of 0.445 m, which is about 17% higher than that accumulated after $A-2$ – the idealised ascending-amplitude load history (0.37 m, which is extracted at the same load level as the ending point of load history $A-1$) if take the displacement after irregular loading as the base (i.e., (0.4451–0.37)/0.445 = 17%). One may assume that representing the irregular load history with idealised regular loading cycles featured as constant average load and load parcels of increasing

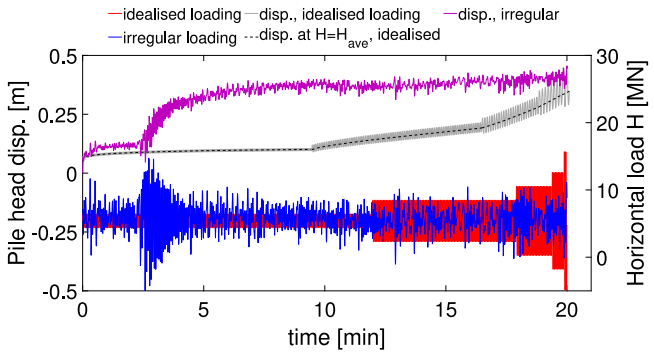

(a) 20m loading history, $H_{peak} = 15.7MN$.

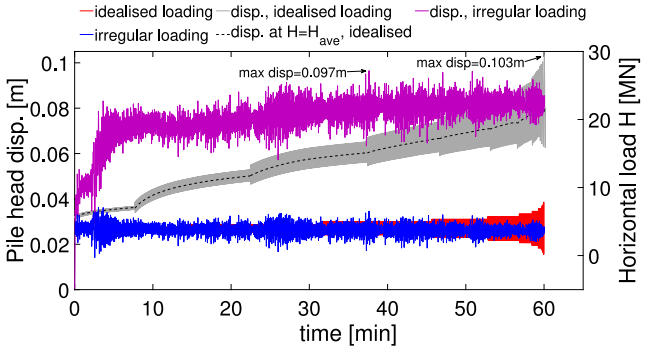

(b) 60m loading history, $H_{peak} = 7.86MN$.

Fig. 14. Pile head displacement evolution: comparison made between irregular loading and idealised regular loading results.

amplitude leads to the conservative estimation of the final accumulated pile displacement. Almost the same maximum pile head displacement for loading cases $A-1$ and $A-2$ (around 0.454 m as indicated in Fig. 14a) occurs near the end of the loading histories — which seems to indicate that the idealisation of the loading history has minor effects on the pile maximum head displacement. To further assess the generality of the two assumptions, the accumulated pile head displacement caused by loading histories $B-1$ and $B-2$ are also investigated.

The loading histories $B-1$ and $B-2$ differ from $A-1$ and $A-2$ on the following aspects: (1) smaller peak loading amplitude (7.86 MN instead of 15.7 MN); (2) longer duration ($A-1$ re-scales the first 20 min of the 1-h storm, $B-1$ contains the complete 1-hour history); and (3) different average load level. However, for $A-1$ and $B-1$, the peak loading amplitude occurs at the same time – $t = 2.5{\sim}2.8$ min. The following observations may be drawn: (1) the accumulated pile head displacements at the end of the two loading histories are almost the same (0.082 m for $B-1$ and 0.08 m for $B-2$) – simulation against idealised loading history no longer show conservatism in this case; (2) the maximum pile head displacement equals 0.097 m for $B-1$ and 0.103 m for $B-2$, which indicates that, similarly to the $A-1-A-2$ simulation, the idealisation of the loading history idealisation has minor effects on the pile maximum head displacement.

Miner's rule and the simulation results (both on monopile in dense and loose sand) in the previous section indicate that pile lateral displacement accumulates rapidly when the load parcel with maximum ever load amplitude is applied. This is demonstrated again by the simulations on the idealised regular loading cases as illustrated in Fig. 14. However, the statement 1 of Miner's rule (which suggests that no displacement is accumulated if the current stress amplitude is smaller than the ever experienced maximum load amplitude) is not fulfilled for monoplie behaviour in dense sand domain. In simulation cases of irregular loading, pile head displacement keeps accumulating after the peak load amplitude being applied.

The maximum load amplitude during the irregular loading $A-1$ occurs at time $t = 2.5{\sim}2.8$ min. However, lateral pile head displacement accumulation keep evolving obviously until $t = 5$ min — after which, the displacement accumulation still continued but with much lower speed. For irregular loading $B-1$, the maximum pile head displacement occurs at $t = 37.6$ min — to compare, the maximum load presents at $t = 2.5{\sim}2.8$ min.

Two possible reasons can lead to this: (1) the ever-changing (which is not significant though) average load level in an irregular load history; (2) duration of the peak load in the irregular load history is too short so that the soil state has not reached its cyclically stable state under such load amplitude levels. The verification (or falsification) of these two assumptions needs further investigations both from experimental and numerical perspectives.

4.2. Soil state around monopile

The study of the distribution of soil relative density and stress state helps to predict long term monopile behaviour from local soil states point of view. Fig. 15a shows the change of relative density D_r in the entire soil domain at the end of the irregular loading storm $B-1$.

Loading $B-1$ is nearly one-way loading with only several minutes' exception. Densification mainly occurs near pile head in front of the loading direction and below pile toe. Fig. 15b indicates that after the idealised loading history $B-2$ being applied, densification occurs at the same location, but also around the middle part of the pile in addition. However, the slightly different soil state in the middle part of the soil seems have minor effects on the pile global tilting: pile head displacement at the end of the loading are quite similar (0.082 m for $B-1$ against 0.08 m for $B-2$) in the two simulation cases.

The stress redistribution (indicated by p/p_{in}) ratio shows greater similarity at the end of the loading $B-1$ (Fig. 16a) and loading $B-2$ (Fig. 16b). Significant increase of p/p_{in} is observed in both cases in front of the loading direction at around $1{\sim}2D$ depth. Mean effective stress reduction occurs in the reverse direction of the loading at shallow layers and in the front direction near pile toe. It should be noticed that such a stress distribution corresponds to nearly one-way cyclic loading event.

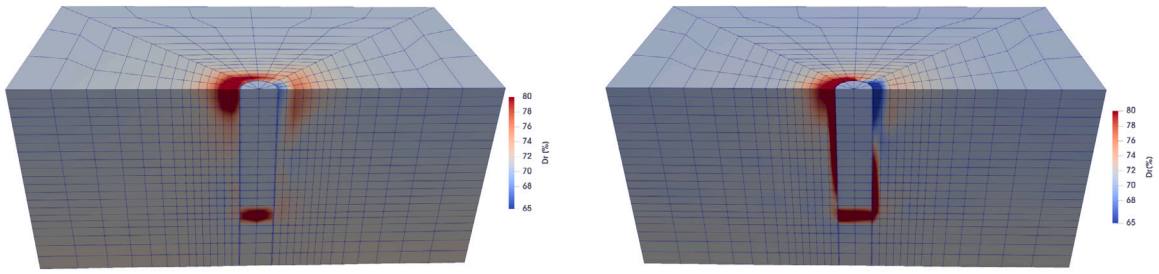

(a) irregular loading $B-1$ (b) idealised regular loading $B-2$

Fig. 15. Relative density D_r at the end of: (a) the irregular loading history $B-1$ and (b) the idealised regular loading history $B-2$.

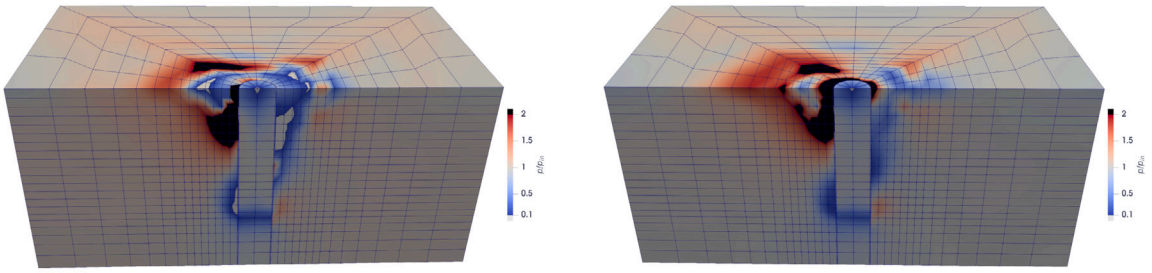

(a) irregular loading $B-1$ (b) idealised regular loading $B-2$

Fig. 16. Distribution of mean effective stress ratio p/p_{in} at the end of: (a) the irregular loading history $B-1$ and (b) the idealised regular loading history $B-2$.

5. Conclusion

In this study, validation of Miner's rule is confirmed at element test level against high-cyclic triaxial test results, under loading conditions of multi-amplitude parcels with different orders. Then, implicit 3D FE modelling was combined with the memory-enhanced, bounding surface SANISANDM-MS model to numerically analyse monopile tilt in dry sand under lateral cyclic loading. Loading cases with regular parcels of multi-amplitude and different parcel sequence are evaluated. Miner's rule is partially validated under drained condition when focusing on the pile head displacement — ordering of loading parcels has minor effects on the accumulated pile head displacement. Monopile response, saying shear force distribution, bending moment distribution and cyclic $p-y$ evolution, is also presented. The similarities observed from the 'Miner' type numerical results between mesoscale (soil stress points) and macroscale (whole soil–pile system) confirm the close link between cyclic soil behaviour and monopile tilting response. Loading idealisation effects on monopile lateral behaviour are studied under conditions of varying load levels and duration. Pile head displacement triggered by irregular and idealised regular loading histories are close to each other, which confirms the validity of using idealised loading history of ascending-amplitude loading parcels to represent for the irregular loading history, in the premise of fully drained condition. Future work will continue to explore the role of relevant geometrical/geotechnical/loading factors, including load multi-directionality and hydromechanical effects related to pore pressure buildup.

Declaration of competing interest

The authors declare that they have no known competing financial interests or personal relationships that could have appeared to influence the work reported in this paper.

Acknowledgement

The authors gratefully acknowledge the support from the Wave Loads and Soil Support for Extra-Large Monopiles (WAS-XL) project (NFR grant 268182).

References

Abadie, C.N., Byrne, B.W., Houlsby, G.T., 2018. Rigid pile response to cyclic lateral loading: laboratory tests. Géotechnique 1–14.

Abadie, C., Byrne, B., Houlsby, G., Burd, H., Mcadam, R., Beuckelaers, W., 2020. Modelling of offshore wind monopile lifetime performance. In: Frontiers in Offshore Geotechnics IV: Proceedings of the 4th International Symposium on Frontiers in Offshore Geotechnics (ISFOG 2020). Taylor & Francis Books Ltd.

Abadie, C.N., Houlsby, G., Byrne, B., 2019. A method for calibration of the hyperplastic accelerated ratcheting model (HARM). Comput. Geotech. 112, 370–385.

Achmus, M., Kuo, Y.-S., Abdel-Rahman, K., 2009. Behavior of monopile foundations under cyclic lateral load. Comput. Geotech. 36 (5), 725–735.

Alonso-Marroquin, F., Herrmann, H., 2004. Ratcheting of granular materials. Phys. Rev. Lett. 92 (5), 054301.

Andersen, K., 2015. Cyclic soil parameters for offshore foundation design. In: Frontiers in Offshore Geotechnics III: Proceedings of the 3rd International Symposium on Frontiers in Offshore Geotechnics (ISFOG 2015), Vol. 1. Taylor & Francis Books Ltd, pp. 5–82.

Arany, L., Bhattacharya, S., Macdonald, J.H., Hogan, S.J., et al., 2015. A critical review of serviceability limit state requirements for monopile foundations of offshore wind turbines. In: Offshore Technology Conference. Offshore Technology Conference.

Barari, A., Bagheri, M., Rouainia, M., Ibsen, L.B., 2017. Deformation mechanisms for offshore monopile foundations accounting for cyclic mobility effects. Soil Dyn. Earthq. Eng. 97, 439–453.

Been, K., Jefferies, M.G., 1985. A state parameter for sands. Géotechnique 35 (2), 99–112.

Bienen, B., Fan, S., Schröder, M., Randolph, M.F., 2021. Effect of the installation process on monopile lateral response. Proc. Inst. Civil Eng. Geotechn. Eng. 1–19.

Byrne, B.W., McAdam, R., Burd, H., Houlsby, G., Martin, C., Zdravkovic, L., Taborda, D., Potts, D., Jardine, R., Sideri, M., et al., 2015. New design methods for large diameter piles under lateral loading for offshore wind applications. Front. Offshore Geotechn. III 705–710.

Corti, R., Diambra, A., Muir Wood, D., Escribano, D.E., Nash, D.F., 2016. Memory surface hardening model for granular soils under repeated loading conditions. J. Eng. Mech. 04016102.

Cuéllar, P., Baeßler, M., Rücker, W., 2009. Ratcheting convective cells of sand grains around offshore piles under cyclic lateral loads. Granul. Matter 11 (6), 379–390.
Cuéllar, P., Mira, P., Pastor, M., Merodo, J.A.F., Baeßler, M., Rücker, W., 2014. A numerical model for the transient analysis of offshore foundations under cyclic loading. Comput. Geotech. 59, 75–86.
Dafalias, Y.F., Manzari, M.T., 2004. Simple plasticity sand model accounting for fabric change effects. J. Eng. Mech. 130 (6), 622–634.
Fan, S., Bienen, B., Randolph, M.F., 2021. Effects of monopile installation on subsequent lateral response in sand. II: Lateral loading. J. Geotech. Geoenviron. Eng. 147 (5), 04021022.
Houlsby, G., Abadie, C., Beuckelaers, W., Byrne, B., 2017. A model for nonlinear hysteretic and ratcheting behaviour. Int. J. Solids Struct. 120, 67–80.
Jostad, H.P., Dahl, B.M., Page, A., Sivasithamparam, N., Sturm, H., 2020. Evaluation of soil models for improved design of offshore wind turbine foundations in dense sand. Géotechnique 70 (8), 682–699.
Jostad, H., Grimstad, G., Andersen, K., Saue, M., Shin, Y., You, D., 2014. A fe procedure for foundation design of offshore structures–applied to study a potential owt monopile foundation in the korean western sea. Geotechn. Eng. J. SEAGS & AGSSEA 45 (4), 63–72.
Kaggwa, W.S., Booker, J.R., Carter, J., 1991. Residual strains in calcareous sand due to irregular cyclic loading. J. Geotech. Eng. 117 (2), 201–218.
Kawamoto, R., Andò, E., Viggiani, G., Andrade, J.E., 2018. All you need is shape: Predicting shear banding in sand with LS-DEM. J. Mech. Phys. Solids 111, 375–392.
Klinkvort, R.T., Hededal, O., 2013. Lateral response of monopile supporting an offshore wind turbine. Proc. ICE-Geotechn. Eng. 166 (2), 147–158.
Klinkvort, R.T., Hededal, O., 2014. Effect of load eccentricity and stress level on monopile support for offshore wind turbines. Can. Geotech. J. 51 (9), 966–974.
Lackenby, J., Indraratna, B., McDowell, G., Christie, D., 2007. Effect of confining pressure on ballast degradation and deformation under cyclic triaxial loading. Géotechnique 57 (6), 527–536.
LeBlanc, C., Byrne, B., Houlsby, G., 2010a. Response of stiff piles to random two-way lateral loading. Géotechnique 60 (9), 715–721.
LeBlanc, C., Houlsby, G.T., Byrne, B.W., 2010b. Response of stiff piles in sand to long-term cyclic lateral loading. Géotechnique 60 (2), 79–90.
Li, W., Igoe, D., Gavin, K., 2015. Field tests to investigate the cyclic response of monopiles in sand. Proc. Inst. Civil Eng. Geotechn. Eng. 168 (5), 407–421.
Liu, H.Y., Abell, J.A., Diambra, A., Pisanò, F., 2019. Modelling the cyclic ratcheting of sands through memory-enhanced bounding surface plasticity. Géotechnique 69 (9), 783–800. http://dx.doi.org/10.1680/jgeot.17.P.307.
Liu, H.Y., Diambra, A., Abell, J.A., Pisanò, F., 2020. Memory-enhanced plasticity modeling of sand behavior under undrained cyclic loading. J. Geotech. Geoenviron. Eng. 146 (11), 04020122.
Liu, H.Y., Kaynia, A.M., 2021. Characteristics of cyclic undrained model SANISAND-MSu and their effects on response of monopiles for offshore wind structures. Géotechnique 1–16.
Liu, H.Y., Kementzetzidis, E., Abell, J.A., Pisanò, F., 2021. From cyclic sand ratcheting to tilt accumulation of offshore monopiles: 3D FE modelling using SANISAND-MS. Géotechnique 1–16.
Liu, H.Y., Pisanò, F., 2019. Prediction of oedometer terminal densities through a memory-enhanced cyclic model for sand. Géotechnique Letters 9 (2), 81–88. http://dx.doi.org/10.1680/jgele.18.00187.
Luo, L., O'Loughlin, C., Bienen, B., Wang, Y., Cassidy, M., Morgan, N., 2020. Effect of the ordering of cyclic loading on the response of suction caissons in sand. Géotechnique Letters 10 (2), 303–310.
Ma, H., Lu, Z., Li, Y., Chen, C., Yang, J., 2021. Permanent accumulated rotation of offshore wind turbine monopile due to typhoon-induced cyclic loading. Mar. Struct. 80, 103079.
McKenna, F., 2011. OpenSees: a framework for earthquake engineering simulation. Comput. Sci. Eng. 13 (4), 58–66.
Miner, M., et al., 1945. Cumulative fatigue damage. J. Appl. Mech. 12 (3), A159–A164.
Page, A.M., Grimstad, G., Eiksund, G.R., Jostad, H.P., 2018. A macro-element pile foundation model for integrated analyses of monopile-based offshore wind turbines. Ocean Eng. 167, 23–35.
Page, A.M., Klinkvort, R.T., Bayton, S., Zhang, Y., Jostad, H.P., 2021. A procedure for predicting the permanent rotation of monopiles in sand supporting offshore wind turbines. Mar. Struct. 75, 102813.
Park, J., Santamarina, J., 2019. Sand response to a large number of loading cycles under zero-lateral-strain conditions: evolution of void ratio and small-strain stiffness. Géotechnique 69 (6), 501–513.
Richards, I.A., Byrne, B.W., Houlsby, G.T., 2019. Monopile rotation under complex cyclic lateral loading in sand. Géotechnique 1–15.
Staubach, P., Machaček, J., Moscoso, M., Wichtmann, T., 2020. Impact of the installation on the long-term cyclic behaviour of piles in sand: A numerical study. Soil Dyn. Earthq. Eng. 138, 106223.
Staubach, P., Machaček, J., Sharif, R., Wichtmann, T., 2021. Back-analysis of model tests on piles in sand subjected to long-term lateral cyclic loading: Impact of the pile installation and application of the HCA model. Comput. Geotech. 134, 104018.
Staubach, P., Wichtmann, T., 2020. Long-term deformations of monopile foundations for offshore wind turbines studied with a high-cycle accumulation model. Comput. Geotech. 124, 103553.
Stewart, H.E., 1986. Permanent strains from cyclic variable-amplitude loadings. J. Geotechn. Eng. 112 (6), 646–660.
Tasiopoulou, P., Chaloulos, Y., Gerolymos, N., Giannakou, A., Chacko, J., 2021. Cyclic lateral response of OWT bucket foundations in sand: 3D coupled effective stress analysis with Ta-Ger model. Soils Found. 61 (2), 371–385.
Truong, P., Lehane, B.M., Zania, V., Klinkvort, R.T., 2019. Empirical approach based on centrifuge testing for cyclic deformations of laterally loaded piles in sand. Géotechnique 69 (2), 133–145. http://dx.doi.org/10.1680/jgeot.17.P.203.
Wichtmann, T., Niemunis, A., Triantafyllidis, T., 2010. Strain accumulation in sand due to drained cyclic loading: on the effect of monotonic and cyclic preloading (Miner's rule). Soil Dyn. Earthq. Eng. 30 (8), 736–745.
Wichtmann, T., Triantafyllidis, T., Chrisopoulos, S., Zachert, H., et al., 2017. Prediction of long-term deformations of offshore wind power plant foundations using HCA-based engineer-oriented models. Int. J. Offshore Polar Eng. 27 (04), 346–356.
Wilkins, E., 1956. Cumulative damage in fatigue. In: Colloquium on Fatigue/Colloque de Fatigue/Kolloquium Über Ermüdungsfestigkeit. Springer, pp. 321–332.
Zografou, D., Gourvenec, S., O'Loughlin, C., 2018. Response of normally consolidated kaolin clay under irregular cyclic loading and comparison with predictions from the accumulation procedure. Géotechnique.